Machine learning approach for full impedance spectrum study of Li-ion battery

1st Cuili Chen
Department of Informatics
Technical University of Munich
Garching by Munich, Germany
cuili.chen@tum.de

2nd Göktug Yesilbas
Department of Informatics
Department of Physics
Technical University of Munich
Garching bei Munich, Germany
g.yesilbas@tum.de

3rd Alexander Lenz
Department of Informatics
Technical University of Munich
Garching bei Munich, Germany
alex.lenz@tum.de

4th Oliver Schneider
Department of Informatics
Technical University of Munich
Garching bei Munich, Germany
oliver_m.schneider@tum.de

5th Alois Christian Knoll
Department of Informatics
Technical University of Munich
Garching bei Munich, Germany
knoll@in.tum.de

***Abstract* — Electrochemical Impedance Spectroscopy (EIS) has been widely applied for Li-ion battery research because EIS can reflect the physical characteristics. The full impedance spectrum sweep generally takes several minutes. Thus, it is impossible to implement a full spectrum sweep for real-time investigations. In this paper, machine learning approach is proposed to address the issue. The proposed approach is based on multi-sine signal sweep technique, where the impedances at corresponding frequencies are derived with a fast Fourier transform. The full impedance spectrum is obtained via machine learning approach. The results are compared with three alternative techniques namely, the piecewise cubic Hermite interpolation polynomial, modified Akima piecewise cubic Hermite interpolation, and Spline. The results demonstrate that the proposed machine learning approach has the best performance.**

Keywords—Li-ion batteries, electrochemical impedance spectroscopy, machine learning, piecewise cubic Hermite interpolation polynomial, modified Akima piecewise cubic Hermite interpolation

I. Introduction

Li-ion batteries (LiBs) are widely adopted in battery electrical vehicles (BEVs) due to their high specific energy, low self-discharge rate, and low cost [1-3]. Even though BEVs are advocated globally due to zero greenhouse gas emission, some limitations of LiBs also impede the broad acceptance of BEVs. One of them is the shorter lifespan compared with fossil fuel vehicles. Intensive research has been carried out to optimize the operation of LiB [4, 5] to prolong the lifespan of BEVs. One of the most prevalent techniques utilized is Electrochemical Impedance Spectroscopy (EIS). This technique is implemented by injecting sinusoidal voltage or current signals to the battery and measuring the corresponding current or voltage signal. The operation of LiBs includes various dynamic processes, such as electron/ion migration, chemical reactions, diffusion in solids/liquids, and relaxation processes [6], whose time constants vary from μs to ms. By injecting sinusoidal signals from mHz to kHz/MHz, the impedance of LiBs can be derived which reflects the physical characteristics [7], ideally permits to separate the electrochemical processes relevant at different time scales, and may be used for operation optimization. Fig. 1 shows the Nyquist plot of a LiB half-cell with the corresponding dynamic processes indicated.

EIS measurements have been utilized to estimate the battery resistance [7, 8], the diffusion coefficient [7], and so on. All of these are vital indicators for the state of health of LiBs [6, 7, 9, 10]. However, due to the large time constant of the diffusion and relaxation processes, the full spectrum EIS measurement takes more than ten minutes which makes it infeasible for online applications. Many approaches have been explored to address this issue. For instance, there is a step pulse technique [11-13] where step pulse acts as incident signal and then a fast Fourier transform (FFT) is applied to derive the full impedance spectra. Single sine injection techniques and multi-sine signal injection techniques (MSSIT) [14, 15] have also been investigated where only characteristics in specified frequency regimes are investigated.

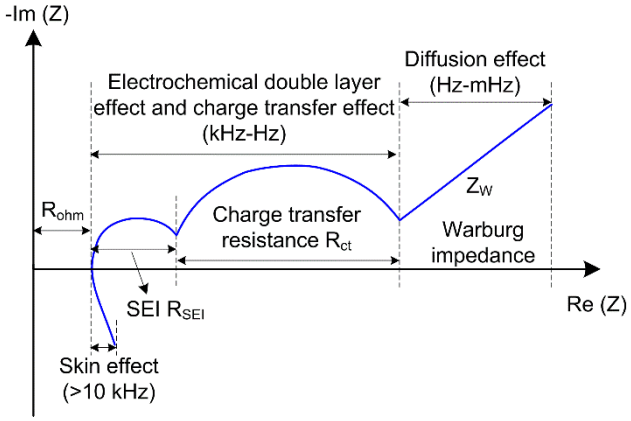

Fig. 1 Schematic Nyquist plot of LiB impedance. SEI: Solid Electrolyte Interface.

This paper examines the role of machine learning (ML) in the EIS analysis. Based on the MSSIT, a ML approach is proposed. This approach is able to provide the full impedance spectra while maintaining the short measurement time of MSSIT. The approach has been applied to both simulation and experimental results. The estimation accuracy is compared with three other techniques, the piecewise cubic Hermite interpolation polynomial (Pchip), modified Akima piecewise cubic Hermite interpolation (Makima), and cubic spline interpolation (spline).

978-1-7281-5414-5/20/$31.00 ©2020 IEEE

The paper is organized as follows. Section II demonstrates the machine learning (ML) approach and three interpolation techniques. Section III illustrates the implementation of the MSSIT based ML in simulation. Experimental results are shown in section IV. Section V is conclusion.

II. The Proposed Machine Learning Approach

A. MSSIT

This paper is based on the MSSIT where multiple sinusoidal current signals with specified frequencies (f_1, f_2, f_3, ⋯, f_n) are injected simultaneously to the battery. The corresponding variation in battery voltage is measured. By FFT, the battery impedance can be derived with (1).

$$Z = \frac{Ue^{jwt+\phi_u}}{Ie^{jwt+\phi_i}} = \frac{U}{I}e^{jwt}e^{\phi_u-\phi_i} = |Z|\,e^{\phi_z} \tag{1}$$

The LiB impedance measurement can be represented with $\{(x_{(i,j)}, y_{(i,j)})$: i=1, 2, …, m. j= 1, 2, …, n.$\}$, where x is the real part of the impedance, y is the imaginary part, i is the number of sample, j is the number of injected sinusoidal signals in each sample. The Nyquist plot of one measurement is illustrated in Fig. 2. It can be noted that a better full spectrum representation can be achieved with more points recorded. However, this also means longer measurement time. Therefore, in multi-sine signal injection, the interpretation of the region between two adjacent points plays a vital role. In this paper, a ML approach is proposed for the interpretation. The theory is illustrated in the following section.

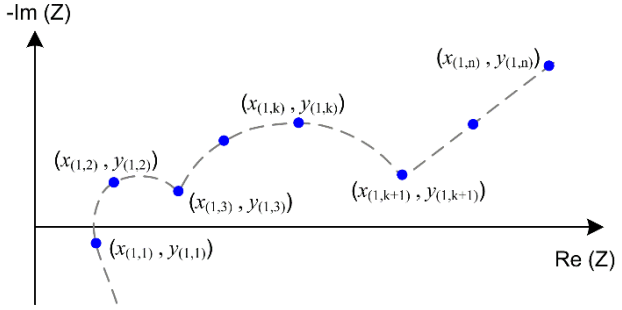

Fig. 2 Schematic Nyquist plot of one LiB impedance measurement. The dotted line represents the full spectrum while the blue circles represent actual data points extracted from MSSIT.

B. Full spectra impedance derivation with ML

Suppose the impedance measurements are collected in a matrix $A_{m\times n}$, where m is number of samples and n is the number of variables. In this case, the variable is frequency. The variables between two adjacent points shown in Fig. 2 are added in the sample as missing values. These m samples include training samples with all variables measured as well as validation samples that have missing variables. The ML algorithm is applied to predict the missing value by low-rank matrix factorization as shown in (2).

$$A \approx LR \tag{2}$$

Where $L_{m\times k}$ and $R_{k\times n}$ are two lower rank matrices, $k \leqslant \min(m, n)$.

The algorithm assigns random values to the matrix $L_{m\times k}$ and $R_{k\times n}$ and finds the best representation of A by minimizing (3).

$$\sum_{i,j|a_{i,j}\neq 0} (l_i^T r_j - a_{i,j})^2 + \lambda\left(\sum_i n_{l_i}\|l_i\|^2 + \sum_j n_{r_j}\|r_j\|^2\right) \tag{3}$$

Where l_i, r_j are the i^{th} row of matrix L and j^{th} column of matrix R respectively. $a_{i,j}$ is the element in i^{th} row and j^{th} column of matrix A. λ is the regularization factor. n_{l_i} is the number of variables for the sample i measured. n_{r_j} is the number of samples that measured this variable j.

C. Polynomial interpolation techniques

The polynomial interpolation techniques have also been applied to find the best representation between data points. Take the k_{th} point (x_k, y_k) and $(k+1)_{th}$ point (x_{k+1}, y_{k+1}) in Fig. 2 as an example, for any $x_k < x < x_{k+1}$, a simple estimation for y is the piecewise linear interpolation as described in (4).

$$f(x) = y_k + (x - x_k)\frac{y_{k+1} - y_k}{x_{k+1} - x_k} \tag{4}$$

In this paper, we investigate Pchip, Makima, and Spline to account for nonlinear characteristics of LiB impedance. All three methods are based on Hermite interpolation as shown in (5).

$$f(x) = \frac{3hs^2 - 2s^3}{h^3}y_{k+1} + \frac{h^3 - 3hs^2 + 2s^3}{h^3}y_k + \frac{s^2(s-h)}{h^2}d_{k+1} + \frac{s(s-h)^2}{h^2}d_k \tag{5}$$

Where d_k and d_{k+1} are the first derivative of $f(x)$ at k and k+1. $h = h_k = x_{k+1} - x_k$, $s = x - x_k$, $\delta_k = (y_{k+1} - y_k)/h_k$.

The three approaches assign different definitions for the first derivatives. In Pchip, the first derivatives are determined so that there is no overshoot in the interpolation between $x_k < x < x_{k+1}$. d_k is assigned to be (6).

$$\frac{w_1 + w_2}{d_k} = \left(\frac{w_1}{\delta_{k-1}} + \frac{w_2}{\delta_k}\right) \tag{6}$$

Where $w_1 = 2h_k + h_{k-1}$, $w_2 = h_k + 2h_{k-1}$.

In Spline, the derivatives are determined by (7).

$$d_{k-1}h_k + 2(h_{k-1} + h_k)d_k + d_{k+1}h_{k-1} = 3(h_k\delta_{k-1} + h_{k-1}\delta_k) \tag{7}$$

The linear equation is then solved to acquire d_k. The main difference between Spline and Pchip lies in the second derivative $f''(x)$, where $f''(x)$ is continuous in Spline but not in Pchip.

In Makima, the first derivatives are derived with (8).

$$d_k = \frac{w_1}{w_1 + w_2}\delta_{k-1} + \frac{w_2}{w_1 + w_2}\delta_k \tag{8}$$

Where w_1 and w_2 are defined below.

$$w_1 = |\delta_{i+1} - \delta_i|, w_2 = |\delta_{i-1} - \delta_{i-2}|.$$

In this paper, the interpolation results are compared with that derived from the ML approach.

III. Simulation Implementation and Analysis

The full spectra impedance derivation is tested by simulation results as well as experimental data. The schematic of the simulation circuit is shown in Fig. 3. The Multi-sine signals are generated by the signal generator to regulate the output of the current source. The frequency of the sinusoidal current varies from 1Hz to 10kHz with an amplitude of 10mA. The current is applied to the battery as excitation signal. Both the applied current I and the battery voltage U are recorded for FFT analysis. The FFT results are then used to derive the battery impedance with the equation (1).

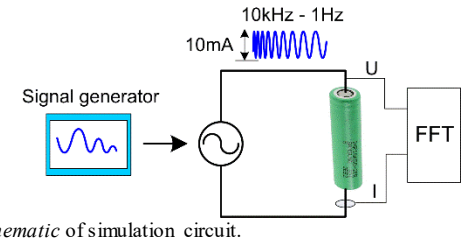

Fig. 3 *Schematic* of simulation circuit.

A. Simulation

In simulation, the battery is modeled with the equivalent circuit shown in Fig. 4 [15]. C_1 is 2mF. C_2 is 160μF. R_1 is 2Ω. R_2 is 2Ω. For full spectrum measurement, ten points per decade are used in the regime between 1Hz and 10kHz. For the multi-sine injection approach, only selected frequencies are injected.

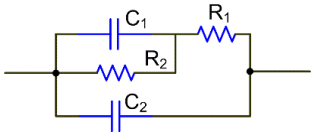

Fig. 4 Equivalent circuit model for LiB.

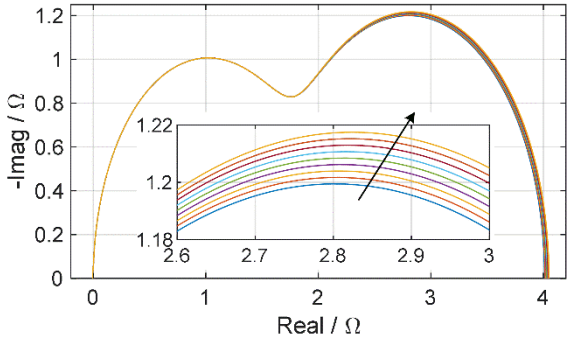

Fig. 5 Nyquist plot of battery impedance in case of R_2 increment (R2 increases from 2Ω to 2.05Ω with even steps).

Fig. 5 demonstrates the change of the full spectra battery impedance in the simulation when the resistor R_2 is varied. There is noticeable increment in the second semicircle of the impedance with the rising of R_2. This imitates the impedance change over time. This means the preferred characteristics at frequency f_1 will shift slightly to a different frequency over time which will lead to inaccurate estimation when MSSIT alone is applied. In this paper, machine learning is proposed to address this issue. The following section illustrates the analysis procedure.

B. Simulation analysis

The battery impedance is divided into three regimes to account for the electron migration, chemical reaction effects. Two validation sets of multi-sine signal tests are carried out. In the first set, the boundary points are selected, while in the second set, the characteristic critical points, which can reflect the shape of the impedance, are selected. Table I gives a summary of the frequency points selected.

Table I Frequencies assigned for two test sets. Unit: Hz.

Set No.	f_1	f_2	f_3	f_4	f_5
1	4k	1.25k	100	1	
2	10k	500	100	25	1

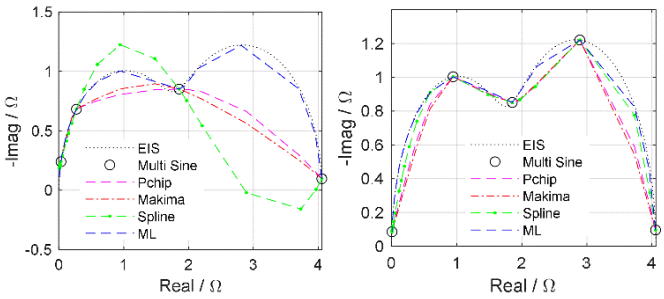

Fig. 6 Comparison of full impedance spectrum constructed with different approaches. (a) MSSIT with boundary points from each regime. (b) MSSIT with characteristic critical points from each regime.

The analysis of the two test sets are shown in Fig. 6a and Fig. 6b, respectively. In the figure, results with 'EIS' legend indicates the impedance measurement obtained by a full spectrum sweep. It can be noted that, even though there are only limited number of data points in MSSIT, with the proposed ML approach, a good reflection of the full spectrum regime can be achieved. For the other three techniques, only when the shape relevant critical points are selected these techniques can provide acceptable results. The impact of the selected points is extraordinary for the Spline approach. Pchip, Makima, and Spline approaches also have a limited performance when it comes to the regime outside the start and the end points.

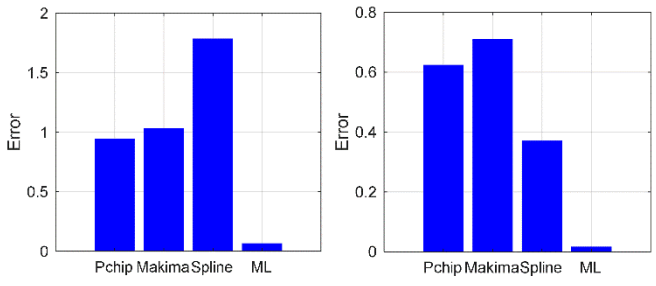

Fig. 7 Estimation error comparison. (a) MSSIT with boundary points from each regime. (b) MSSIT with characteristic critical points from each regime.

The squared error between the EIS measurements and the estimations from Pchip, Makima, Spline, and the proposed ML approach are compared in Fig. 7a and Fig. 7b. Traditional approaches, such as Pchip, Makima, and Spline, are excessively influenced by the selected frequencies in the MSSIT approach, while the ML approach shows good performance at both conditions. Similar characteristics have been observed for experimental results and are discussed in the following section.

IV. Experimental Test and Full Spectrum Derivation

This section specifies the practical test conditions and demonstrates the comparison of full spectrum derivation between the four approaches, ML, Pchip, Makima, Spline.

A. Test design

In the experiment, a Sony US18650FT (K C1113ZK08J, rated capacity: 1.1 Ah) is tested with a Gamry Interface 5000P. Firstly, the battery is pre-discharged and characterized at 1C. Then, the battery is cycled at 4C charging and discharging rate for 210 cycles. For the first ten cycles, EIS measurements are conducted after each cycle. These data are used as training samples. Afterwards, EIS measurements are carried out every

ten cycles. These are the validation data. All the EIS measurements are carried out at 100% state of charge (SoC) and in the regime between 10mHz and 20kHz. In total, there are 10 samples as training data and 20 samples as validation data.

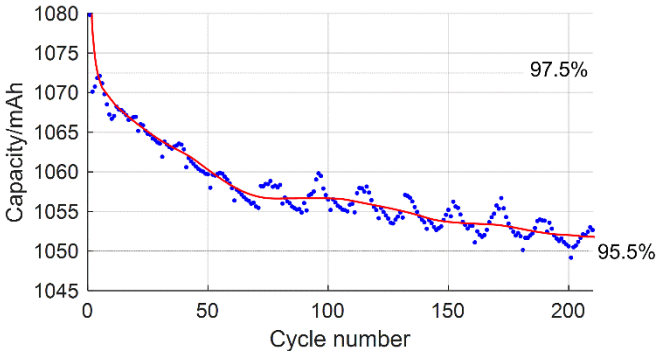

Fig. 8 Capacity degradation over cycling with 4C charging and discharging rate.

Fig. 8 shows the capacity loss during the power cycling process. In average, the capacity reduces from 97.5% of rated capacity to about 95.5% by the end of the power cycling. A maximum capacity of 1080mAh is reached. This capacity is smaller than rated capacity, it can be due to fast charging rate and the calendar aging (the battery was stored about one year at room temperature before the power cycling test.).

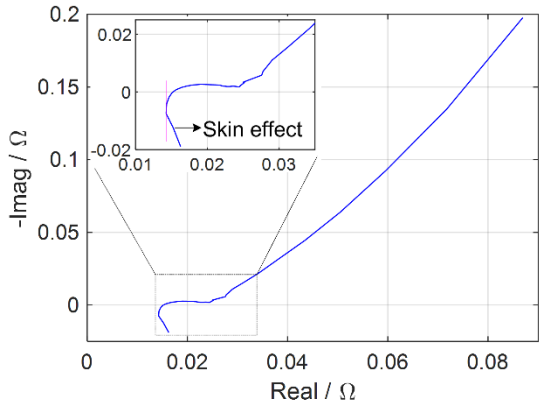

Fig. 9 Impedance spectra of the battery cell at 100% SoC in the first cycle.

Fig. 9 shows the EIS measurement in the first cycle. In this test, the skin effect occurs between 3kHz and 20kHz. The internal resistance is 15.2 mΩ at about 1kHz. Then, the semi-circle is caused by processes like electrochemical double layer charging and charge transfer. Finally, the Warburg impedance, which is caused by diffusion, appears in the mHz regime. Since the skin effect appears at high frequency regime, and it contributes less to the total time cost of the EIS measurement compared with other characteristics in the impedance spectra, the analysis in the following section is focused between 20mHz and 2kHz.

B. *Derivation of full spectrum*

In order to derive the full impedance spectra, several points are selected from the EIS measurement as the results from MSSIT. The selected frequency points are shown in Table II. The first data set includes all the boundary points corresponding to the electron migration, chemical reaction, and diffusion phenomena, while the second data set covers the major characteristic critical points. The selected points are then utilized for full spectra derivation.

Table II Frequencies selected for two test sets. Unit: Hz.

Set No.	f_1	f_2	f_3	f_4	f_5
1	1.979k	200.9	4.971	0.020	
2	1.979k	200.9	4.971	2.020	0.020

Fig. 10 shows the derivation results for cycle 20, which is the first sample in the validation data set. It compares the derivation results by four different techniques, Pchip, Makima, Spline, ML, with the EIS measurements and selected Multi-sine measurements. Fig. 10a and Fig. 10b are the results with the first and the second data set, respectively. In both cases, Pchip, Makima and ML techniques have stable estimation, while the spline approach is strongly influenced by the selected data points, and its estimation accuracy increased when the characteristic critical points were selected. In all these approaches, ML techniques reveal the best performance.

Fig. 11 illustrates the RMS error of the four techniques applied to twenty validation data sets. It shows that the proposed ML technique has the best accuracy and the estimation error is stable over the twenty samples. The RMS error of the Spline approach fluctuates a lot especially with the characteristic critical data set. In the author's opinion, this is because the Spline technique depends on the data points, a shift caused by the degradation will introduce a large variance in the estimation results. Spline is more suitable for MSSIT with dense sampling points.

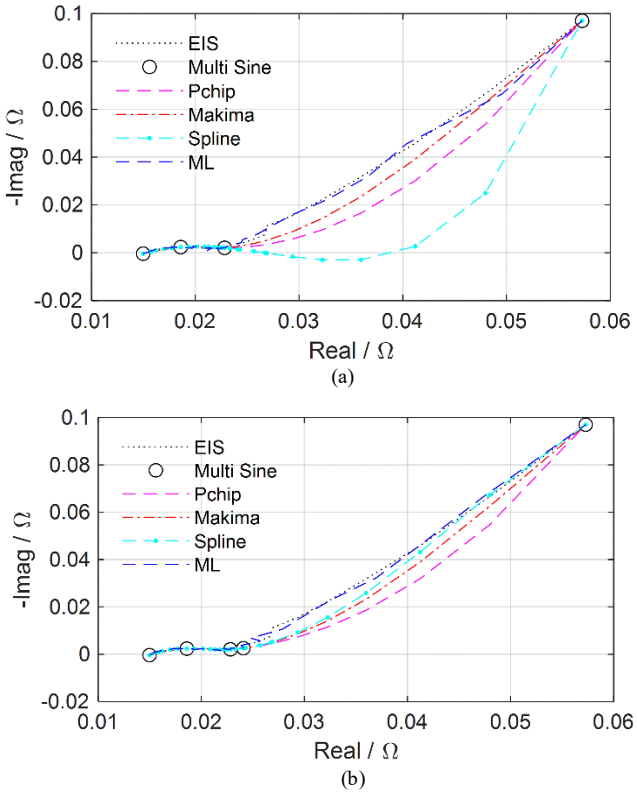

Fig. 10 Comparison of full impedance spectrum derivation from experimental results. (a) MSSIT with boundary points from each regime. (b) MSSIT with characteristic critical points from each regime.

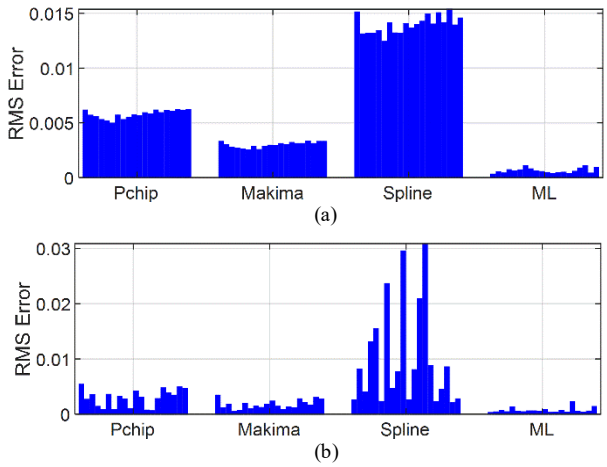

Fig. 11 RMS error of all validation data sets. (a) MSSIT with boundary points from each regime. (b) MSSIT with characteristic critical points from each regime.

C. *Estimation over power cycling*

The derivation results over power cycling have also been investigated. Fig. 12 displays the impedance in the 1st, 50th, 120th, 190th power cycle corresponding to the first training sample and the fourth, eleventh, and eighteenth validation sample. In general, the impedance derived from multi-sine measurement points can reflect the characteristics of the full impedance spectra. This is mainly due to the fact that the machine learning approach has included the operation history in the analysis and thus is able to incarnate the characteristics with the aging effect. The reconstructed impedance with ML is able to distinguish between the impedance in 1st, 50th, 120th, and 190th power cycle.

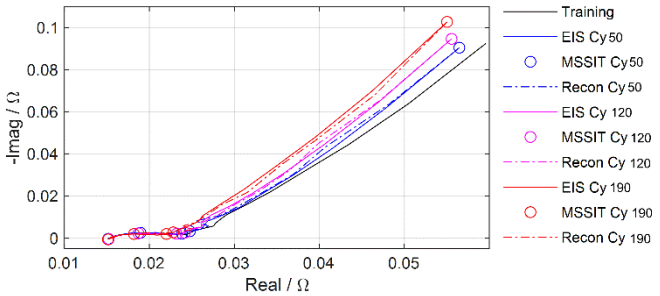

Fig. 12 Impedance derivation with ML over power cycling. Training: first sample in the training dataset. EIS CyXX: EIS measurement in cycle XX. MSSIT CyXX: MSSIT measurement in cycle XX. Recon CyXX: reconstructed impedance with ML in cycle XX.

V. Conclusion

EIS is a good technique to study the battery performance. However, the implementation of the technique is time consuming. In this paper, a machine learning approach is proposed to shorten the measurement time. The approach is based on multi-sine signal injection approach, but it compensates the drawback so that full impedance spectra are captured in the frequency domain even though only selected points are measured. The results are compared with three other approaches, the piecewise cubic Hermite interpolation polynomial, a modified Akima piecewise cubic Hermite interpolation, and Spline. The results show that machine learning approach outperforms the other approaches and is not dependent on the sampling points used in the multi-sine signal sweep technique.

The proposed machine learning approach has also been applied to power cycling tests on Sony cell. The proposed approach is able to distinguish different power cycles. More research will be carried out to improve the accuracy of the proposed technique.

Acknowledgment

This work was funded by the German Ministry of Education and Research (Bundesministerium für Forschung und Bildung, BMBF) within the NOVBATCON project (reference no. 16EMO0319), which is gratefully acknowledged. Our gratitude also goes to colleagues from VDI / VDE Innovation + Technik GmbH for their support in the project.

References

[1] C. Pillot, "The worldwide battery market 2012-2025," presented at the BATTERIES 2013, Nice, FRANCE, October 14 -16, 2013, 2013.

[2] J. M. Amanor-Boadu, A. Guiseppi-Elie, and E. Sánchez-Sinencio, "Search for Optimal Pulse Charging Parameters for Li-Ion Polymer Batteries Using Taguchi Orthogonal Arrays," *IEEE Transactions on Industrial Electronics,* vol. 65, no. 11, pp. 8982-8992, 2018, doi: 10.1109/TIE.2018.2807419.

[3] U. Consortium. "Electric Vehicle Battery Test Procedures Manual." (accessed).

[4] C. F. Zou, X. S. Hu, Z. B. Wei, T. Wik, and B. Egardt, "Electrochemical Estimation and Control for Lithium-Ion Battery Health-Aware Fast Charging," (in English), *Ieee Transactions on Industrial Electronics,* Article vol. 65, no. 8, pp. 6635-6645, Aug 2018, doi: 10.1109/tie.2017.2772154.

[5] N. Tian, H. Fang, and Y. Wang, "Real-Time Optimal Lithium-Ion Battery Charging Based on Explicit Model Predictive Control," *IEEE Transactions on Industrial Informatics,* pp. 1-1, 2020, doi: 10.1109/TII.2020.2983176.

[6] S. Solchenbach, D. Pritzl, E. J. Y. Kong, J. Landesfeind, and H. A. Gasteiger, "A Gold Micro-Reference Electrode for Impedance and Potential Measurements in Lithium Ion Batteries," *J. Electrochem. Soc.,* vol. 163, no. 10, pp. A2265-A2272, January 1, 2016 2016, doi: 10.1149/2.0581610jes.

[7] X. Wang, X. Wei, and H. Dai, "Estimation of state of health of lithium-ion batteries based on charge transfer resistance considering different temperature and state of charge," *J. Energy Storage,* vol. 21, pp. 618-631, 2019/02/01/ 2019, doi: https://doi.org/10.1016/j.est.2018.11.020.

[8] P. Vyroubal and T. Kazda, "Equivalent circuit model parameters extraction for lithium ion batteries using electrochemical impedance spectroscopy," *J. Energy Storage,* vol. 15, pp. 23-31, 2018/02/01/ 2018, doi: https://doi.org/10.1016/j.est.2017.10.019.

[9] H. Yuan and L. Dung, "Offline State-of-Health Estimation for High-Power Lithium-Ion Batteries Using Three-Point Impedance Extraction Method," *IEEE Transactions on Vehicular Technology,* vol. 66, no. 3, pp. 2019-2032, 2017, doi: 10.1109/TVT.2016.2572163.

[10] E. Din, C. Schaef, K. Moffat, and J. T. Stauth, "A Scalable Active Battery Management System With Embedded Real-Time Electrochemical Impedance Spectroscopy," *IEEE Transactions on Power Electronics,* vol. 32, no. 7, pp. 5688-5698, 2017, doi: 10.1109/TPEL.2016.2607519.

[11] J. A. A. Qahouq and Z. Xia, "Single-Perturbation-Cycle Online Battery Impedance Spectrum Measurement Method With Closed-Loop Control of Power Converter," *IEEE Transactions on Industrial Electronics,* vol. 64, no. 9, pp. 7019-7029, 2017, doi: 10.1109/TIE.2017.2686324.

[12] Z. Xia and J. A. A. Qahouq, "Method for online battery AC impedance spectrum measurement using dc-dc power converter duty-cycle control," in *2017 IEEE Applied Power Electronics Conference and Exposition (APEC)*, 26-30 March 2017 2017, pp. 1999-2003, doi: 10.1109/APEC.2017.7930973.

[13] D. A. Howey, P. D. Mitcheson, V. Yufit, G. J. Offer, and N. P. Brandon, "Online Measurement of Battery Impedance Using Motor Controller Excitation," *IEEE Transactions on Vehicular*

Technology, vol. 63, no. 6, pp. 2557-2566, 2014, doi: 10.1109/TVT.2013.2293597.

[14] H. Zappen, F. Ringbeck, and U. D. Sauer, "Application of Time-Resolved Multi-Sine Impedance Spectroscopy for Lithium-Ion Battery Characterization," *Batteries,* vol. 4, no. 4, 2018, doi: 10.3390/batteries4040064.

[15] B. Bullecks, R. Suresh, and R. Rengaswamy, "Rapid impedance measurement using chirp signals for electrochemical system analysis," *Comput. Chem. Eng.,* 10.1016/j.compchemeng.2017.05.018 vol. 106, pp. 421-436, // 2017, doi: 10.1016/j.compchemeng.2017.05.018.